Continental Shelf Research 30 (2010) 1211–1225

Contents lists available at ScienceDirect

Continental Shelf Research

journal homepage: www.elsevier.com/locate/csr

Impacts of freshwater on the seasonal variations of surface salinity and circulation in the Caspian Sea

A. Birol Kara [a], Alan J. Wallcraft [a,*], E. Joseph Metzger [a], Murat Gunduz [b]

[a] Oceanography Division, Naval Research Laboratory, Stennis Space Center, MS, USA
[b] Institute of Marine Sciences, Middle Eastern Technical University, Erdemli, Icel, Turkey

ARTICLE INFO

Article history:
Received 21 July 2008
Received in revised form
23 March 2010
Accepted 29 March 2010
Available online 2 April 2010

Keywords:
Caspian Sea
Heat flux
Freshwater flux
The Volga River
HYCOM

ABSTRACT

A fine resolution (≈ 3.3 km) version of the HYbrid Coordinate Ocean Model (HYCOM) is developed for the Caspian Sea. The model consists of a hybrid $\sigma - z$ coordinate system, with σ−coordinates for the upper layers and z-levels below a user-specified depth and in very shallow water. General features of the Caspian Sea HYCOM are presented including the bottom topography, initialization and atmospheric forcing along with river discharge. The climatologically forced model simulation reveals that there is net heat loss (gain) during winter (summer), and that rivers can have significant influence on the freshwater fluxes, especially on the northwestern shelf. There is a strong seasonal cycle in the net surface heat fluxes. The freshwater fluxes are found to be locally dominated by river discharge. In particular, the Volga River, which has very high discharge rate during the summer months, is found to play an important role in driving the seasonal cycle of freshwater fluxes in the North Caspian Sea. Over the basin, the buoyancy fluxes calculated from net heat and freshwater fluxes indicate that buoyancy is much more sensitive to variations in heating than precipitation–evaporation since thermal buoyancy fluxes are much greater than the haline buoyancy fluxes. A set of model simulations further investigates the impact of evaporation, precipitation and river flow on the upper ocean quantities. It is demonstrated that the discharge rate from the Volga River controls the monthly variations in surface salinity fields in the North Caspian Sea.

Published by Elsevier Ltd.

1. Introduction

The Caspian Sea has several unique characteristics, making it a very challenging enclosed body of water for examining seasonal variations of upper ocean variables. It consists of three distinct basins (north, central and south regions), having their own physical conditions and biological diversity (Fig. 1). The northern part of the Caspian Sea covers about 25% of the total surface area. The Caspian Sea has no connection to any other major ocean basin. Upper ocean variables, such as surface salinity and currents, are therefore locally influenced by the seasonally varying impacts of river discharge, evaporation and precipitation in addition to heat and momentum fluxes. Long-term climatic effects are of particular importance in the Caspian Sea as well. For example, Rodinov (1994) relates variations in sea level to cycles of North Atlantic Oscillation (NAO).

There are many small and large rivers (nearly 130), but the majority of them have small discharge rates. The largest inflow of fresh water comes from the Volga River (Fig. 1). It accounts for about 80% of the climatological mean river discharge of $\approx 250\,km^3\,yr^{-1}$ (Kosarev and Yablonskaya, 1994). The outflow in the Caspian Sea is mainly by evaporation at the sea surface and to Kara-Bogaz. The sea level in the Caspian Sea displays a clear seasonal cycle, generally reaching its lowest seasonal value in winter and increasing during May–July, following the spring floods (e.g., Domroes et al., 1998). Thus, it is mainly a function of evaporation–precipitation (Rodinov, 1994) and these local effects can be important in predicting the upper ocean variables.

The Northern Caspian Sea is very shallow, with average depths shallower than 5 m. Having a large extent of shallow water over most of the coastal regions in the Caspian Sea points to the importance of properly representing stratification and mixing processes, which can be influenced by atmospheric forcing. Since greater constraints need to be imposed in the formulation of boundary fluxes in an enclosed basin in comparison to a semi-enclosed or open ocean, improperly accounting for mass or buoyancy fluxes could lead to unrealistic estimates of total stored heat, salt and mass in a numerical ocean model of the Caspian Sea.

Despite its small size, the above mentioned factors make the Caspian Sea a challenging region to investigate the impact of various variables, such as river discharge, heat and freshwater fluxes, on the seasonal variations of salinity. There are several

* Corresponding author.
E-mail addresses: alan.wallcraft@nrlssc.navy.mil (A.J. Wallcraft), joe.metzger@nrlssc.navy.mil (E. Joseph Metzger), gunduz@ims.metu.edu.tr (M. Gunduz).
URL: http://www.7320.nrlssc.navy.mil (A.J. Wallcraft).

0278-4343/$ - see front matter Published by Elsevier Ltd.
doi:10.1016/j.csr.2010.03.011

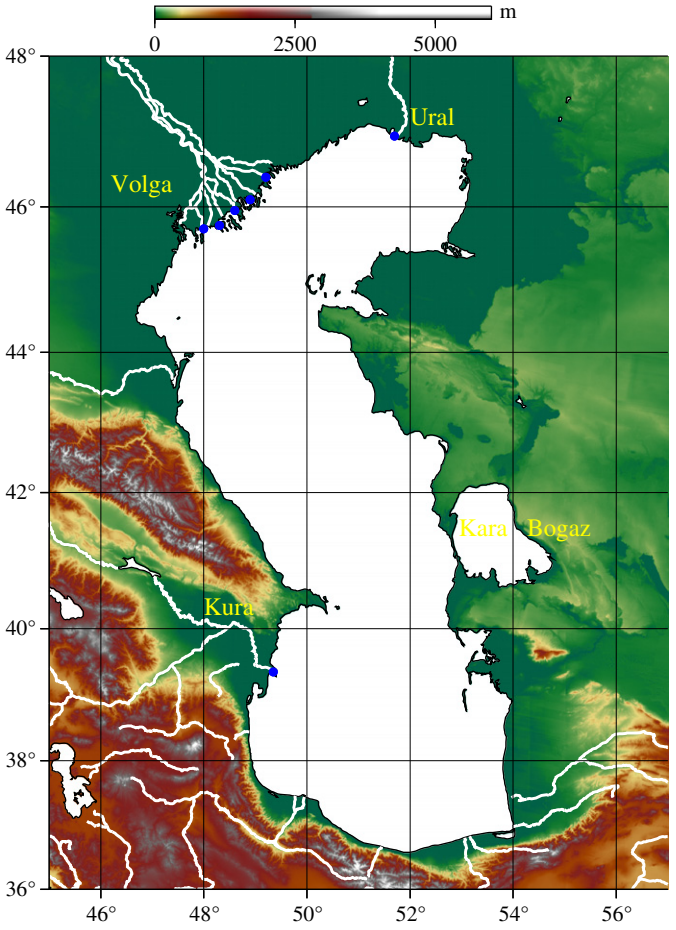

Fig. 1. The geography of the Caspian Sea. Locations of the major rivers discharged into the Caspian Sea are also provided. The length of the coastline is ≈7000 km, and the surface area is 386,400 km^2.

operational atmospheric models from which heat and freshwater fluxes at the sea surface can be obtained. Examples of such models include $1.125^\circ \times 1.125^\circ$ resolution European Centre for Medium-Range Weather Forecasts (ECMWF) 40-year Re-Analyses (ERA-40) and $1.875^\circ \times 1.875^\circ$ resolution National Centers for Environmental Predictions (NCEP) Re-Analysis. On the other hand, their grid resolutions are too coarse to resolve many small scale features for the relatively small Caspian Sea which is $\approx 4^\circ$ in width. For this reason, the use of much finer horizontal resolution products is of particular importance. In addition, the general circulation in the Caspian Sea is reported to be cyclonic based on both indirect estimates of currents (floats, bottles or dynamical methods), and a few hydrodynamic interpretations (Terziev et al., 1992; Bondarenko, 1993). However, results from these studies are limited in time and space. Thus, there is lack of information about upper ocean quantities in the Caspian Sea, making an eddy-resolving ocean model essential to examine the spatial and temporal variability of various variables over the seasonal cycle.

Given the lack of reliable eddy-resolving numerical ocean models for investigating the main oceanographic features in the Caspian Sea, including their dynamical and physical processes, there is a strong motivation to develop one, which is one major focus of this study. Therefore, we introduce a fine resolution Caspian Sea model and use it to study the main oceanic features in the region. The model combines the advantages of different coordinate systems within a single framework to allow for the optimal coordinate choice in simulating coastal and open ocean features in the Caspian Sea. Along these lines, the main objectives of this paper are to examine (1) the general and mesoscale ocean circulation features over the seasonal cycle, and (2) the impact of rivers, evaporation, precipitation and salt fluxes on the sea surface salinity (SSS).

2. Caspian Sea HYCOM

While a fine resolution ocean model is essential due to reasons mentioned above, at present, the enclosed Caspian Sea is a forgotten component of a global ocean system. It is included neither in high resolution eddy resolving ocean models nor in existing operational models. Examples of such fine resolution models are provided in Table 1. In addition, the existing modeling studies in the Caspian Sea have been limited in scope. Earlier studies used shallow water and diagnostic models, which have very coarse resolutions (e.g., Shkudova, 1973).

Here, we introduce a HYbrid Coordinate Ocean Model (HYCOM) configured for the Caspian Sea. The model is based on a primitive-equation formulation (Bleck, 2002). It contains five prognostic equations: two for the horizontal velocity components, a mass continuity or layer thickness tendency equation and two conservation equations for a pair of thermodynamic variables, such as salt and potential temperature or salt and potential density.

HYCOM uses a generalized (hybrid isopycnal/terrain-following (σ)/z-level) coordinate system. In particular, it behaves like a conventional σ (terrain-following) model in very shallow oceanic regions, like a z-level (fixed-depth) coordinate model in the mixed layer or other unstratified regions, and like an isopycnic-coordinate model in stratified regions (e.g., Bleck, 2006). The model uses the layered continuity equation to make a dynamically smooth transition to z-levels in the unstratified surface mixed layer and σ—levels in shallow water. The optimal coordinate is chosen at every time step using a hybrid coordinate generator. The model presented here is a stand-alone ocean model with no assimilation of any ocean data, including SST, and no relaxation to any other data except SSS to keep salinity balance on track as will be explained later.

2.1. General features

The Caspian Sea HYCOM is set up with a grid resolution of $1/25^\circ \cos(\text{lat}) \times 1/25^\circ$ (latitude × longitude) on a Mercator grid. Zonal and meridional array sizes in the model are 354 and 204, respectively. The Mercator grid has square cells with a resolution of $0.04 \times \cos(\text{lat}) \times 111.2$ km. This corresponds to 3.5 km resolution at the southern regions (at 38°N) and 3.1 km resolution at the northern regions (at 46°N). Thus, the average grid resolution can be considered as ≈3.3 km.

Table 1
Examples of OGCMs excluding the Caspian Sea.

Resolution	OGCM	Reference
1/32°	NRL Layered Ocean Model (NLOM)	Shriver et al. (2007)
1/16°	Mediterranean Forecasting System (MFSTEP)	Pinardi et al. (2003)
1/12°	Danish Meteorological Institute (DMI)	Buch and She (2005)
1/12°	HYbrid Coordinate Ocean Model (HYCOM)	Wallcraft et al. (2008)
1/8°	Navy Coastal Ocean Model (NCOM)	Barron et al. (2006)
1/3°	MERCATOR	Ferry et al. (2007)
1°	Forecasting Ocean Assimilation Model (FOAM)	Bell et al. (2006)

The model is configured with 30 vertical $\sigma-z$ (hybrid) layers. In water deeper than 55 m, the top layer is 1 m thick and each subsequent layer is 1.1898 × thicker than the one above to form a set of z-levels with the 14th interface at 55 m and, at the deepest point, the 29th interface at 809 m with the bottom at 1010 m. The scale factor of 1.1898 is chosen to get 30 layers to cover about 1000 m. In water between 55 and 11 m deep, only the top 14 layers are active and they are all scaled by the depth to form a terrain-following $\sigma-$coordinate. For example, if the depth is 27.5 m (11 m) the top layer is 50 cm (20 cm) thick. Shallower than 11 m, the coordinate switches back to z-level with the top layer now always 20 cm thick. This configuration is depicted in Fig. 2, which shows the flat z-levels in deep water, the $\sigma-$coordinate over the shelf, and flat z-levels again in the shallow water north of 45°N. Note that HYCOM's hybrid coordinate allows partial cells (i.e., the bathymetry can take any value, not just z-levels), and that layers below the bottom are actually treated as zero thickness layers. This does not affect the solution, but it means that all 30 layers are included in the computation at all sea points.

The Caspian Sea HYCOM simulations use realistic bottom topography constructed from a local data set (Ibrayev, personal communication, 2007). After interpolation to the model grid, the final topography was smoothed twice with a 9-point smoother (Fig. 3). This was necessary to reduce topographic energy generation at small scales poorly resolved by the model. The Northern Caspian Sea is relatively shallow with an average depth of approximately <5 m, gradually deepening towards the interior. In the central region, depths are typically >500 m.

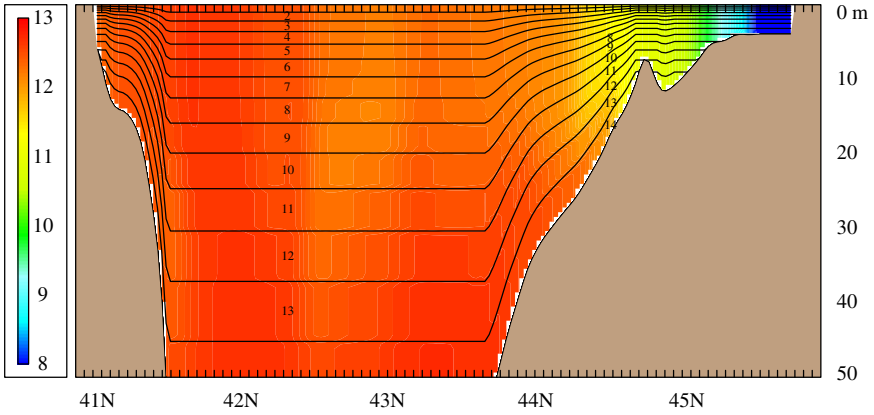

Fig. 2. Meridional cross-section of climatological mean salinity (psu) in August from the eddy-resolving 3.3 km resolution HYCOM simulation at 49.28°E. Layer numbers in the model are also provided. In the figure only the top 14 layers are shown.

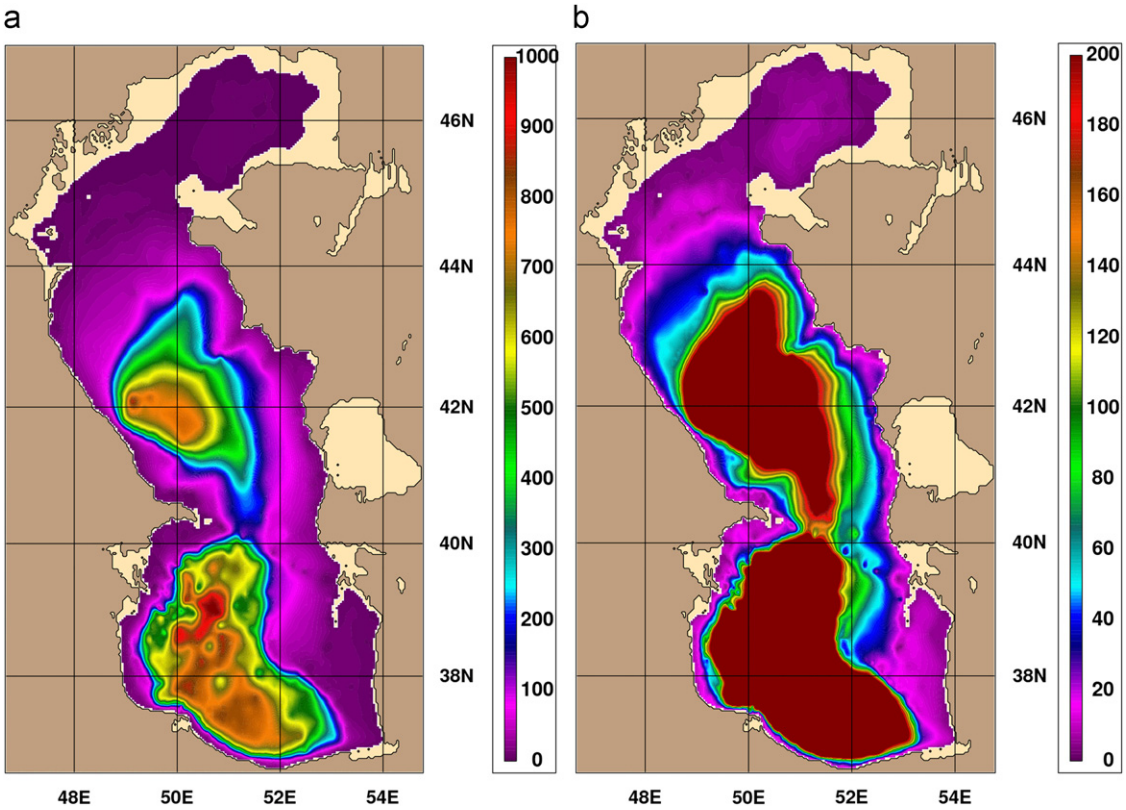

Fig. 3. Bottom topography (m) of the Caspian Sea. The model land-sea boundary is set at 2 m and shown in light tan. (a) Full bathymetry (m) and (b) Shallow regions (m).

The southern basin is the deepest part in the region with a maximum depth of 1010 m. Having such topographical features makes the Caspian Sea an ideal laboratory as a test-bed region for studying the combined effects of coastal and open ocean processes.

The mean sea level is set at −27.9 m, with the model coastline at the 2 m isobath (i.e., at −29.9 m) and all depths between 2 and 4 m changed to 4 m. The value of −27.9 m is representative of yearly Caspian Sea level time series. Some small inland water regions along with Kara-Bogaz are shown in light tan in Fig. 3. These areas are excluded from the model domain because using the 2 m isobath as the coastline, they had no connection to the main body of water and thus would have little effect on the basin as a whole. A standard thermodynamic energy-loan ice model is included in HYCOM. Since it is not a dynamic ice model, the ice does not move with the wind and ocean currents. However, HYCOM does include the effects of ice formation and melting on SSS.

2.2. Model initialization

The Caspian Sea HYCOM is initialized using monthly mean temperature and salinity climatologies obtained from Ibrayev et al. (2001). The original resolution of these climatologies is $0.25^{\circ} \times 0.20^{\circ}$. The vertical depth levels are at 0, 5, 10, 15, 20, 25, 30, 50, 75, 100, 125, 150, 200, 250, 300, 400, 500, 600, 800. For simplicity we only show the basin-averaged temperature and salinity profiles extending down to 500 m (Fig. 4). The Caspian Sea has very low salinity (fresh to 12–13 psu), which is about a third the typical salinity of seawater (35 psu). In deep waters, salinity varies little with depth (Kosarev and Tuzhilkin, 1995). Temperature gradually drops with depth, while salinity is constant $\approx$11.8 psu below 50 m. HYCOM's equation of state is a relatively low order polynominal, cubic in temperature and quadratic in salinity, that has been optimized for potential temperature in the range −2 to 40 °C and salinity in the range 18–38 psu. Fortunately, this polynominal happens to also be a good fit to the equation of state near 12 psu. However, at 0 psu the potential density is typically 0.05–0.1 kg m^{-3} too high or the equivalent of a salinity difference of about 0.06–0.12 psu. This level of difference is negligible relative to other factors in the simulation.

In the model there is a relaxation to monthly mean SSS climatology of Ibrayev et al. (2001) to prevent drift in time and to keep the salinity balance on track. Based on several tests, the reference mixed layer thickness for the SSS relaxation is 30 m (30 days in 30 m e-folding time). The actual e-folding time depends on the mixed layer depth (MLD) and is 30 days × MLD/30 m, i.e., it is more rapid when the MLD is shallow and less so when it is deep. The effective e-folding time is shorter, i.e., effective relaxation is stronger for shallower MLD. The coefficient of relaxation is constant, but its effect depends on the MLD.

2.3. Atmospheric forcing and river inflow

HYCOM reads in the following time-varying atmospheric forcing fields: wind forcing (zonal and meridional components of wind stress, wind speed at 10 m above the sea surface) and thermal forcing (air temperature and air mixing ratio at 2 m above the sea surface, precipitation, net shortwave radiation and net longwave radiation at the sea surface). Monthly climatological means of these wind and thermal atmospheric forcing variables were formed based on 6 hourly data from ERA-40 (Uppala et al., 2005). The years prior to 1979 were not used in computing the means since there was relatively little data assimilated into the ERA-40 re-analysis before this time. Thus, monthly mean climatologies are constructed during the time period of September 1979–August 2002. For the model simulations, 6 hourly intra-monthly anomalies are added to the monthly wind climatologies. Details of adding anomalies are described in an earlier study by Kara et al. (2005a).

The model treats rivers as a runoff addition to the surface precipitation field. The flow is first applied to a single ocean grid point and smoothed over surrounding ocean grid points, yielding a contribution to precipitation in m s^{-1}. There are three major rivers used in the model simulations, and these are the Volga, Kura and Ural. Note that the Volga River discharges into the Caspian Sea at five locations. Monthly mean discharge rates for

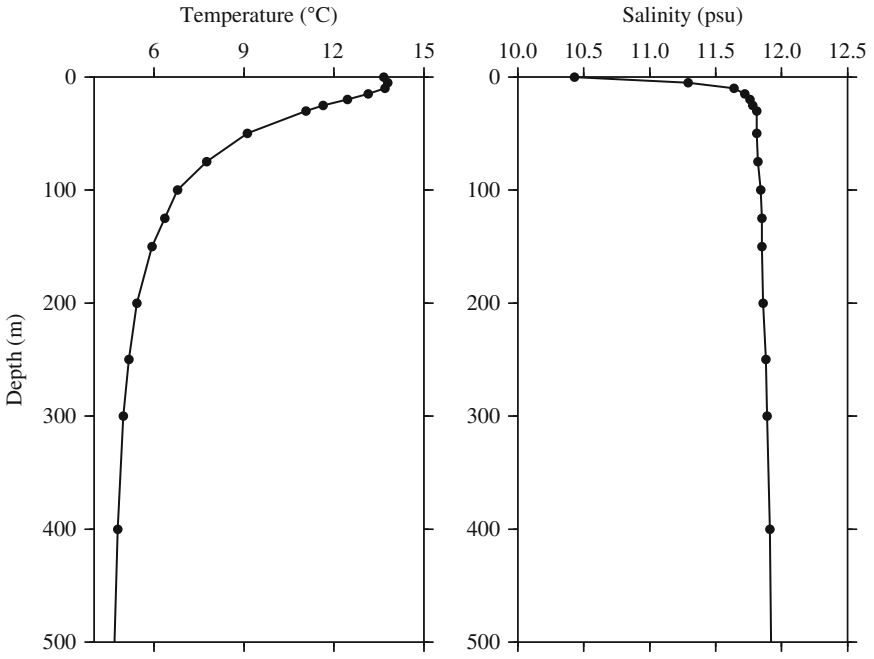

Fig. 4. Annual mean of basin-averaged temperature (°C) and salinity (psu) profiles in the Caspian Sea. Taken from the Ibrayev et al. (2001) climatology.

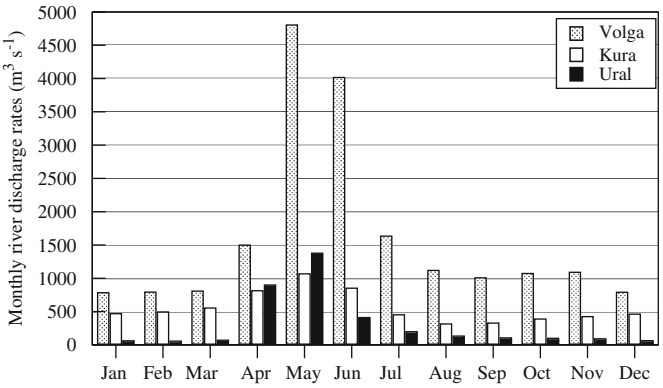

Fig. 5. Monthly mean discharge rates ($m^3 s^{-1}$) from the NRL data set for the major rivers discharged into the Caspian Sea. In the NRL river climatology the monthly stream flow numbers are obtained from the RivDIS data set (http://www.daac.ornl.gov/daacpages/rivdis.html). For the Volga River, discharge rates are equal for each month for A–E.

each river are provided in Fig. 5. They are obtained from the Naval Research Laboratory (NRL) river discharge climatology (Barron and Smedstad, 2002).

2.4. HYCOM simulations

The model first ran for 5 years until statistical equilibrium was reached and then extended for another 4 years. The same climatological atmospheric forcing was used for the entire 9-year simulation. A linear regression analysis was performed for domain averaged quantities (layer temperature, salinity, potential and kinetic energy, etc.) to investigate statistical equilibrium in each layer. The Caspian Sea HYCOM is deemed to be in statistical equilibrium when the rate of potential energy change is acceptably small (e.g., $<1\%$ in 5 years) in all layers.

There are several mixed layer sub-model options in HYCOM. Their implementation, details and evaluations are presented in Halliwell (2004) and Kara et al. (2008). In all Caspian Sea HYCOM simulations presented in this paper, the K-profile parameterization (KPP) of Large et al. (1997) is used. Investigating the impact of various mixing schemes is beyond the focus of this paper.

All model results presented in the following sections are based on either daily or monthly means that were constructed from the last 4 years of the simulations. At least a 4-year mean was needed because the eddy-resolving 3.3 km resolution Caspian Sea HYCOM is non-deterministic due to flow instabilities at this resolution. Note that performing a 1-month (1 year) HYCOM Caspian Sea simulation takes $\approx$45 min (9 h) on 64 HP/Compaq SC45 processors.

3. Upper ocean variables in the Caspian Sea

3.1. Sea surface circulation

The knowledge about the surface circulation features in the Caspian Sea is very limited. Only a small amount of observations near the coastal regions exists. The sea surface circulation based on the available data is described in an earlier study by Kosarev and Yablonskaya (1994). That study explains that surface winds are primarily responsible for controlling the sea surface circulation in the Northern Caspian Sea. Satellite altimeter data could be used to examine if HYCOM is able to reproduce the observed sea level variability, and thus provide a measure of the realism of the circulation. However, that is beyond the scope of this paper and a topic of future study.

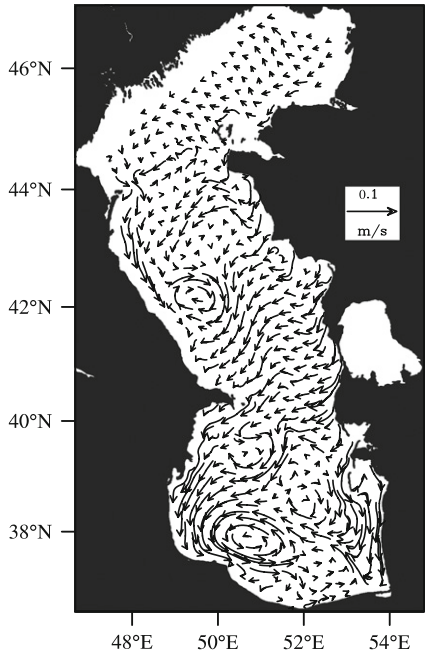

Fig. 6. Annual mean surface currents obtained from the 3.3 km resolution climatologically forced Caspian Sea HYCOM simulation. The length of the reference velocity vector is 10 cm s^{-1}. The annual mean was formed using model years 5–8. The reader is cautioned that the current vectors obtained from the 3.3 km resolution HYCOM are not plotted at each individual model grid point since there are to many of them, affecting the clarity of the plot. Instead, we sub-sample the current vectors.

Annual mean sea surface currents from the Caspian Sea HYCOM simulation are shown in Fig. 6. The climatological annual mean is obtained by averaging currents over all days using the last four model years. Previously, Kosarev and Yablonskaya (1994) revealed the existence of southward currents along the western part of the basin in the mid-Caspian Sea, a feature evident in the HYCOM simulation as well. One of the most distinct features noted from Fig. 6 is that there are generally weak (strong) currents in the north (south). In particular, currents can be a weak as a few cm s^{-1} in the north, while they can reach a strength of tens of cm s^{-1} in the south.

Seasonal variations of sea surface currents reveal the existence of a few well-organized eddies over the basin (Fig. 7). These are located near the southwestern coast and western side of the central region over a majority of the months. A few meanders, small coastal eddies and dipole structures are also noted. The Rossby radius of deformation in the Caspian Sea is $\approx 15-20$ km (e.g., Baidin and Kosarev, 1986). Thus, the radii of coastal eddies in the model can be a few multiples of the radius of deformation. These eddies are especially prevalent in the western part of region. The circulation in the mid-Caspian Sea is generally cyclonic during winter. There are also strong coastal currents flowing along the southeasternmost coast of the region.

In the central Caspian Sea, the circulation is mostly cyclonic (southward current along the western coast and northward current along the eastern coast) during winter (e.g., in January). Beginning in February, a southward current starts to develop along the eastern coast of the sea. There is generally a very strong Ekman current flowing from the eastern side of the sea to the interior associated with the upwelling along the eastern side during summer. This is always evident in June, July and August. Such currents are also noted in September and October and can reach to the western coast of the southern basin. Another striking pattern evident from monthly surface currents is the anticyclonic

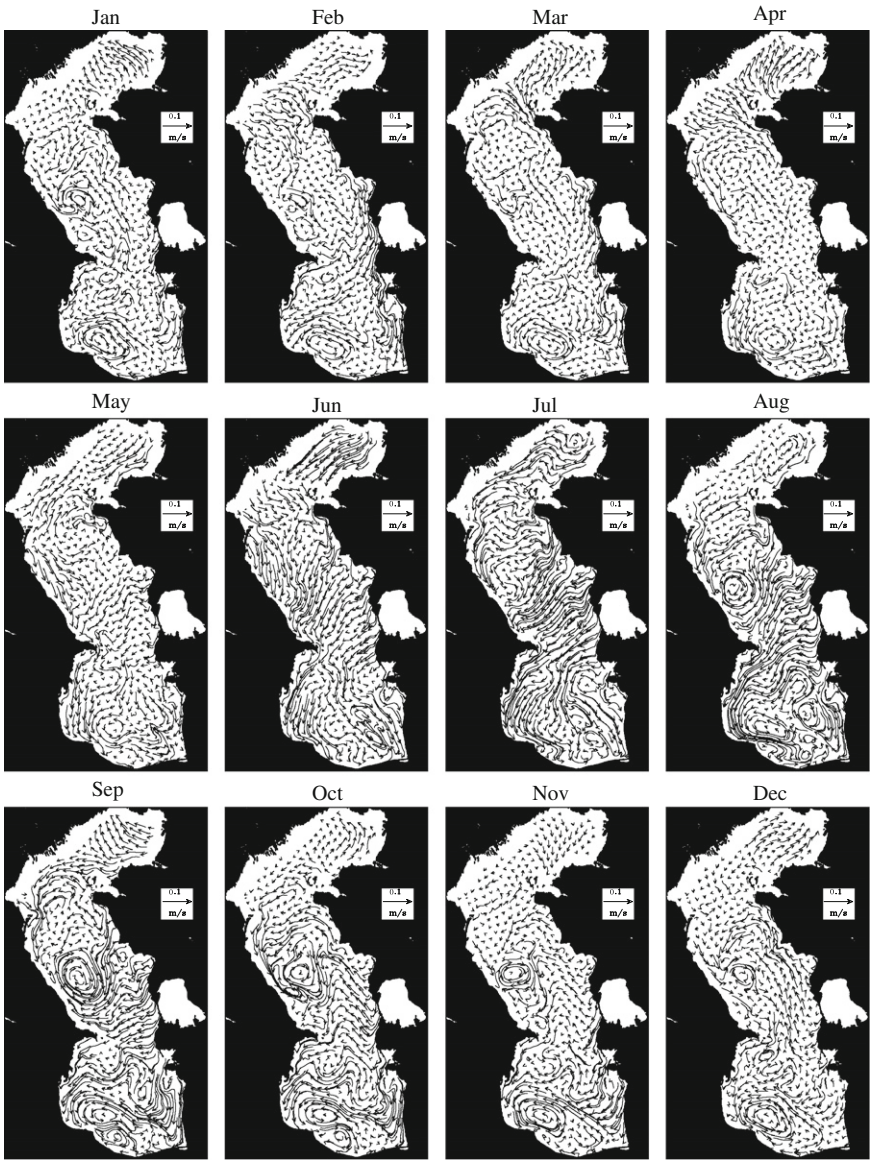

Fig. 7. Monthly mean surface currents obtained from the 3.3 km resolution climatologically forced Caspian Sea HYCOM simulation. The length of the reference velocity vector is 10 cm s^{-1}. As in Fig. 6, the velocity vectors are sub-sampled for plotting purposes.

circulation in the interior of the central Caspian Sea. This anticyclonic gyre begins to develop in August and preserves its structure until the end of the December. Since the gyre is located over the deep depression of the bathymetry there, it is speculated that this feature is strongly controlled by bathymetry. There is no clear evidence of its existence based on the available observational data.

In the Southern Caspian Sea, there is a cyclone centered near (38°N,51°W). The intensity of this gyre is stronger during winter. There is a southward current along either side of the Southern Caspian Sea, and the intensity of currents along the eastern coast weakens in winter months. However, starting from August these currents become more intense. Previously, Knysh et al. (2008) have also used an ocean model to examine the seasonal circulation dynamics of the Caspian Sea. Consistent with that study, the southward current in the western region is evident from the HYCOM simulation as well. The southward current along the eastern coast of the South Caspian Sea is also revealed by both models. HYCOM also shows a persistent cyclonic circulation centered at ($\approx$38°N,51°W) over the southernmost part of the Caspian Sea in May, in agreement with the one reported by Knysh et al. (2008). However, the location of the gyre in HYCOM is displaced a little bit to the north.

3.2. Heat and freshwater fluxes

In this section, seasonal variations of the net heat and freshwater fluxes at the sea surface are examined, along with their contributions to buoyancy fluxes. For simplicity, only monthly means will be shown. However, basin averages of daily fluxes will also be presented to demonstrate high frequency variations in these fields.

Before presenting results, we first provide a summary of how these fluxes are computed in the eddy-resolving Caspian Sea HYCOM. The net surface heat flux that has been absorbed (or lost) by the upper ocean is parameterized as the sum of the downward shortwave radiation, upward longwave radiation and the downward latent and sensible heat fluxes. Details of these computations are provided in the Appendix. Net freshwater flux is

expressed as P–E, where P is the precipitation due to rain ($m\,s^{-1}$), and E is the evaporation ($m\,s^{-1}$). Note that P–E is multiplied by water density to have the flux form (see below) so it has units of $kg\,m^{-2}\,s^{-1}$. However, only the flux's effect on salinity is included. E is calculated using simulated latent heat flux based on model SST at each time step. In other words, E is not a prescribed forcing and is computed as $E = Q_L/(\rho_w L)$ where Q_L is latent heat flux ($W\,m^{-2}$), ρ_w is water density ($1022\,kg\,m^{-3}$), and L is latent heat of vaporization ($L = (2.501 - 0.00237 \times SST)10^6\,J\,kg^{-1}$). P is directly obtained from ERA-40. Both net heat and freshwater fluxes at the sea surface are defined as positive quantities into the ocean.

Following the traditional formulation of Gill (1982), the total buoyancy flux (B_f) which is the sum of thermal and haline buoyancy fluxes is parameterized as follows:

$$B_f = \underbrace{-\frac{g}{\rho_0}\left[\frac{\alpha(T_s,S_s)Q_a}{C_w}\right]}_{\text{Thermal buoyancy flux}} + \underbrace{\frac{g}{\rho_0}[\rho_0\beta(T_s,S_s)(E-P)S_s]}_{\text{Haline buoyancy flux}}, \quad (1)$$

$$\alpha(T_s,S_s) = \frac{-\partial\rho/\partial T}{\rho_0}, \quad (2)$$

$$\beta(T_s,S_s) = \frac{\partial\rho/\partial S}{\rho_0}, \quad (3)$$

where g is the gravitational acceleration ($9.81\,m\,s^{-2}$), T_s is the model SST (°C), $\alpha(T_s,S_s)$ is the thermal expansion coefficient ($^\circ C^{-1}$), $\beta(T_s,S_s)$ is the salinity expansion coefficient (psu^{-1}), S_s is the SSS (psu), ρ is the water density ($kg\,m^{-3}$), ρ_0 is the reference density ($1000\,kg\,m^{-3}$), Q_a is the net heat flux at the sea surface ($W\,m^{-2}$) and C_w is the specific heat of water ($3993\,J\,kg^{-1}\,K^{-1}$). The expansion coefficients for temperature and salinity are calculated from the equation of state (Brydon et al., 1999), and by convention, are both defined to be positive.

The buoyancy flux in Eq. (1) involves both the thermal and haline buoyancy fluxes. In our case, the haline buoyancy includes both the conventional P–E and relaxation to climatological SSS and river runoff. Positive (negative) buoyancy flux indicates a buoyancy loss (gain). Surface density increases (i.e., the water column is destabilized) if $B_f > 0$, and surface density decreases (i.e., water column is stabilized) if $B_f < 0$.

Net heat and freshwater fluxes along with the components of total buoyancy fluxes reveal strong seasonal variations in the Caspian Sea (Fig. 8). In all panels, positive (negative) values are in red (blue). As evident from the net surface heat fluxes, heat loss occurs in January, March, September and November (i.e., during winter and fall), and associated with high solar heating there is always heat gain in the other months. The net heat gain is largest ($> 200\,W\,m^{-2}$) in the easternmost part of the region in July when the coastal upwelling generally occurs. Unlike the net surface heat

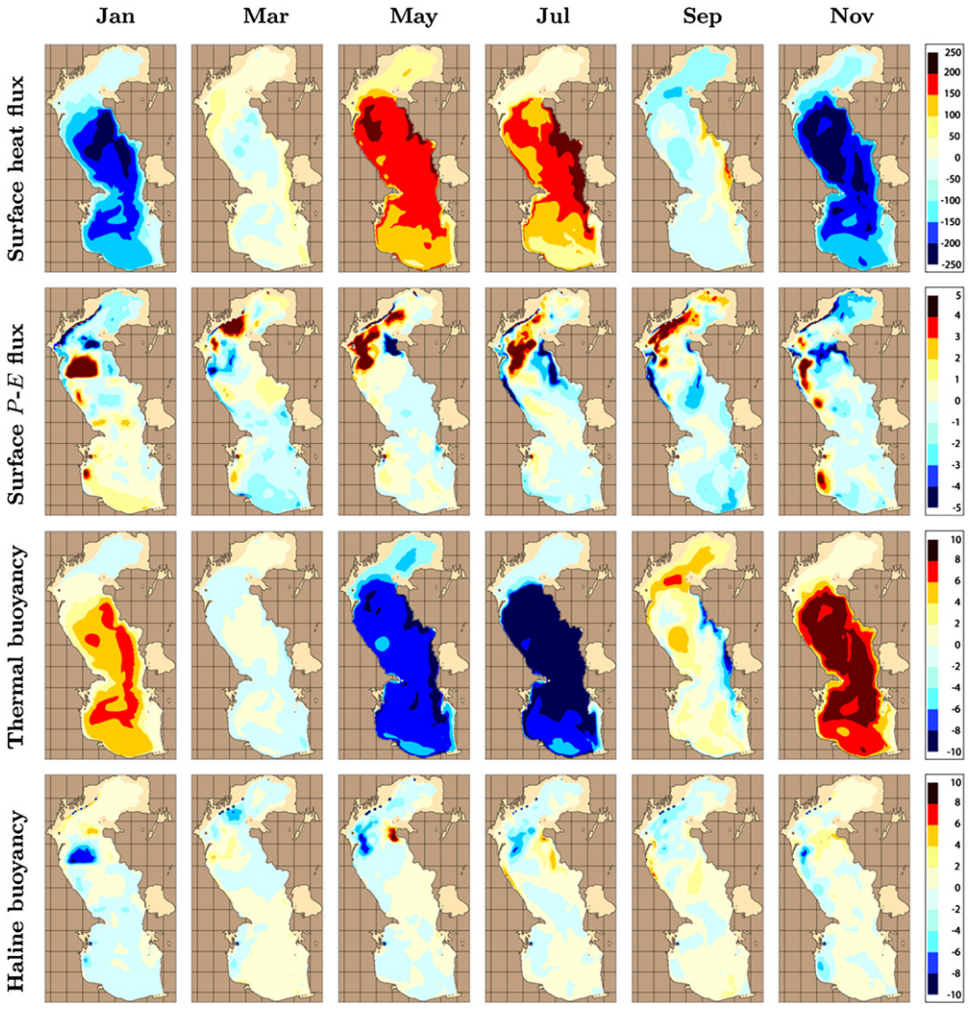

Fig. 8. Spatial variations of net surface heat flux ($W\,m^{-2}$), net surface freshwater flux ($\times 10^{-4}\,kg\,m^{-2}\,s^{-1}$), thermal and haline buoyancy fluxes ($\times 10^{-8}\,m^2\,s^{-3}$). Climatological monthly means are obtained from the eddy-resolving Caspian Sea HYCOM simulation. For convenience the panels are shown for every other month. Note that the scale of the color palette for both thermal and haline buoyancy fluxes is the same.

flux which is relatively homogeneous on monthly time scales, there can be both positive and negative freshwater fluxes in the Caspian Sea for a given month. From the definition, having positive $P–E$ values (i.e., $P > E$) implies precipitation dominating over evaporation, typically resulting in production of freshwater stratification. This is usually seen in the North Caspian Sea, and especially near the Volga River from March to September. The impact of $P–E$ on the salinity of the region is discussed in Section 4 in detail.

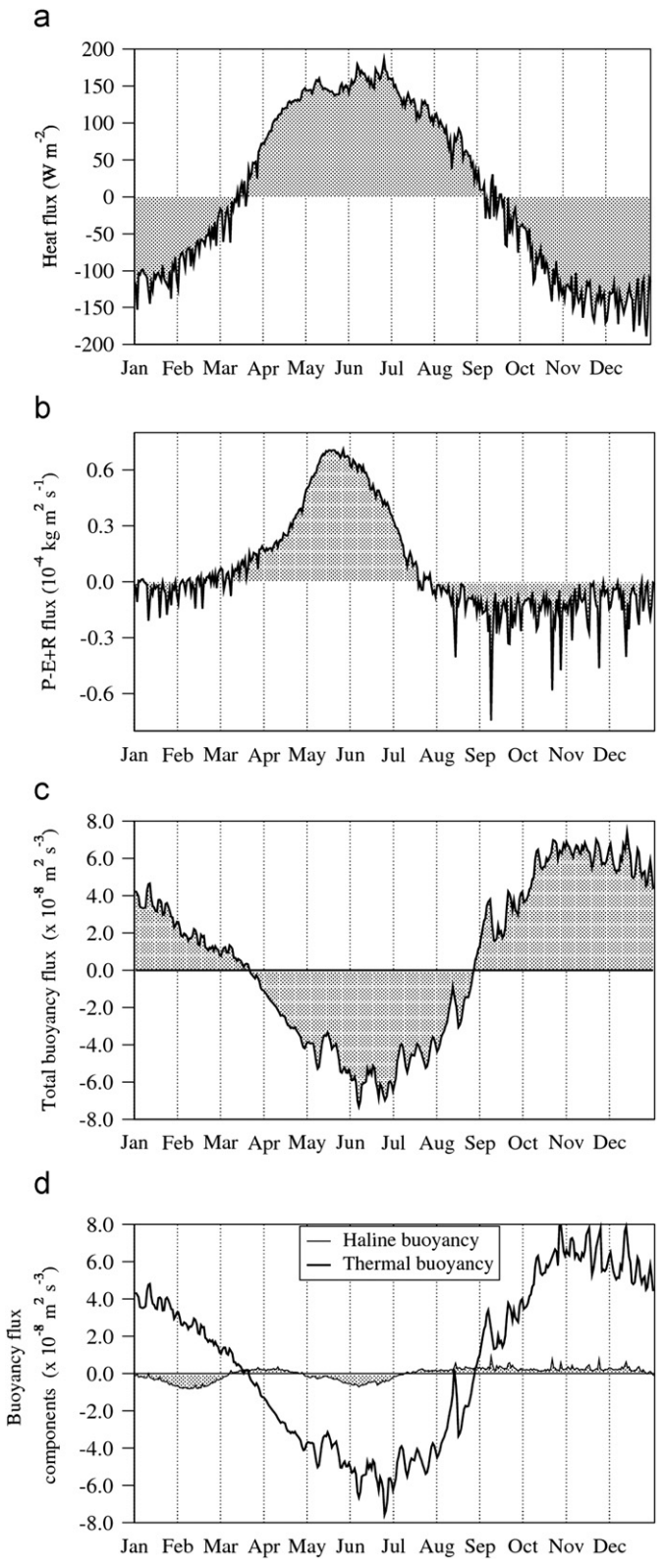

Fig. 9. Basin-averaged climatological daily mean of surface fluxes obtained from the Caspian Sea HYCOM simulation: (a) net heat flux ($\mathrm{W\,m^{-2}}$), (b) net $P–E+R$ flux (including river runoff but excluding relaxation to surface salinity) ($\times 10^{-4}\,\mathrm{kg\,m^{-2}\,s^{-1}}$), (c) total buoyancy flux ($\times 10^{-8}\,\mathrm{m^2\,s^{-3}}$) and (d) thermal and haline buoyancy fluxes ($\times 10^{-8}\,\mathrm{m^2\,s^{-3}}$).

The thermal buoyancy flux is much larger than the haline buoyancy flux over most of the Caspian Sea (Fig. 8). Therefore, the buoyancy is much more sensitive to variations in heating. Unlike the net heat fluxes, positive buoyancy flux (i.e., the regions in red) results in a buoyancy loss so thermal buoyancy fluxes indicate a gain in May and July. Therefore, it can be stated that thermal buoyancy flux stabilizes the upper ocean during these particular time periods. Monthly mean haline buoyancy values are almost identical for each month. In almost half of the region, the haline buoyancy flux indicates a gain. This is typical in the majority of months. One can also notice that while thermal buoyancy flux generally dominates the haline buoyancy flux, locally there are regions where the reverse is true. For example, the buoyancy is mostly influenced by the freshwater fluxes on the shelf near the Volga River.

To provide general information about how heat and freshwater fluxes vary over the Caspian Sea, basin averages of these variables are computed. This is done based on daily averaged values, so that high temporal variations in these variables can be seen (Fig. 9a, b). In response to the solar heating, the strong seasonal cycle is evident from the net heat fluxes at the sea surface. Net heat gain starts in mid-March and continues through September. Net surface heat flux reaches a maximum value of $\approx 200\,\mathrm{W\,m^{-2}}$ during June–July. The basin-averaged daily mean net precipitation–evaporation+runoff also reveals a seasonal cycle with maximum values in late spring/early summer. This maximum is associated with river runoff (Fig. 5).

Similar to net heat and freshwater fluxes, basin averages of total buoyancy flux along with its components are examined (Fig. 9c, d). The shaded regions in the plots denote time periods when there is a buoyancy gain or loss. Accordingly, there is buoyancy gain starting from the end of March through the end of August (Fig. 9c). This is also reflected in the thermal buoyancy flux which dominates the haline buoyancy (Fig. 9d).

4. Impacts of evaporation, precipitation and rivers

In addition to the standard simulation which has been used in the analyses so far, we performed four additional Caspian Sea HYCOM simulations (Table 2). The purpose of having these simulations is to examine the impact of SSS relaxation, $P–E$ and rivers on the upper ocean surface circulation and salinity. In brief, as analyzed in the earlier sections, expt. 1 is the standard simulation that includes SSS relaxation, $P–E$ forcing and river forcing. In expt. 2, there is no SSS relaxation; otherwise, it is identical to expt. 1. Thus, expt. 2 is taken as a "default" simulation since $P–E$ and rivers are included. Differences between expt. 1 and expt. 2 provide the impacts of SSS relaxation. The remaining simulations are based on expt. 2 which has no SSS relaxation. In particular, expt. 3 is twin of expt. 2 but there is no $P–E$ forcing, and expt. 4 is twin of expt. 2 but there is no river forcing. Finally, expt. 5 excludes SSS relaxation, $P–E$ forcing and river forcing, i.e., zero salt flux at the sea surface.

Monthly means of sea surface circulation are already introduced in Section 3.1 (see Fig. 7) and taken as reference plots to compare with those from the additional simulations listed in Table 2. To demonstrate seasonal differences in the surface currents among the simulation expts. of 2–5, monthly means are plotted for February and August, and annual means averaged all

over the months are also included (Fig. 10). Surface circulation from all simulations reveal similar features, and generally agrees with the standard simulation shown in Fig. 7. This is true for the annual mean, and in the February and August means as well.

The river runoff has little influence on the surface currents in the interior. Note that comparing surface currents from atmospherically forced eddy resolving ocean models may be problematic in some cases because eddies are not a direct response to the atmospheric forcing. The eddy field can be different in two simulations with identical forcing due to mesoscale flow instabilities. In our case, using the same atmospheric forcing (i.e., ERA-40), the surface circulation from all simulations is mostly identical. This also indicates that the change in the forcing (i.e., *P–E* and rivers being turned off) did not have any significant effects on the surface circulation.

Table 2
Descriptions of Caspian Sea HYCOM simulations.

Simulation	SSS relaxation	*P–E*	Rivers
Expt. 1	On	On	On
Expt. 2	Off	On	On
Expt. 3	Off	Off	On
Expt. 4	Off	On	Off
Expt. 5	Off	Off	Off

Table 3
Vector correlations for surface currents computed between the standard simulation and each of the others.

SSS relaxed	Default	No *P–E*	No Rivers	No salt flux
Jan.	0.86	0.92	0.77	0.90
Feb.	0.91	0.94	0.85	0.93
Mar.	0.88	0.94	0.78	0.91
Apr.	0.89	0.94	0.79	0.91
May	0.94	0.96	0.89	0.94
Jun.	0.97	0.98	0.94	0.97
Jul.	0.97	0.98	0.96	0.98
Aug.	0.94	0.98	0.91	0.96
Sep.	0.94	0.98	0.92	0.96
Oct.	0.94	0.97	0.87	0.95
Nov.	0.92	0.97	0.97	0.94
Dec.	0.89	0.96	0.77	0.93
Ann.	0.97	0.99	0.92	0.97

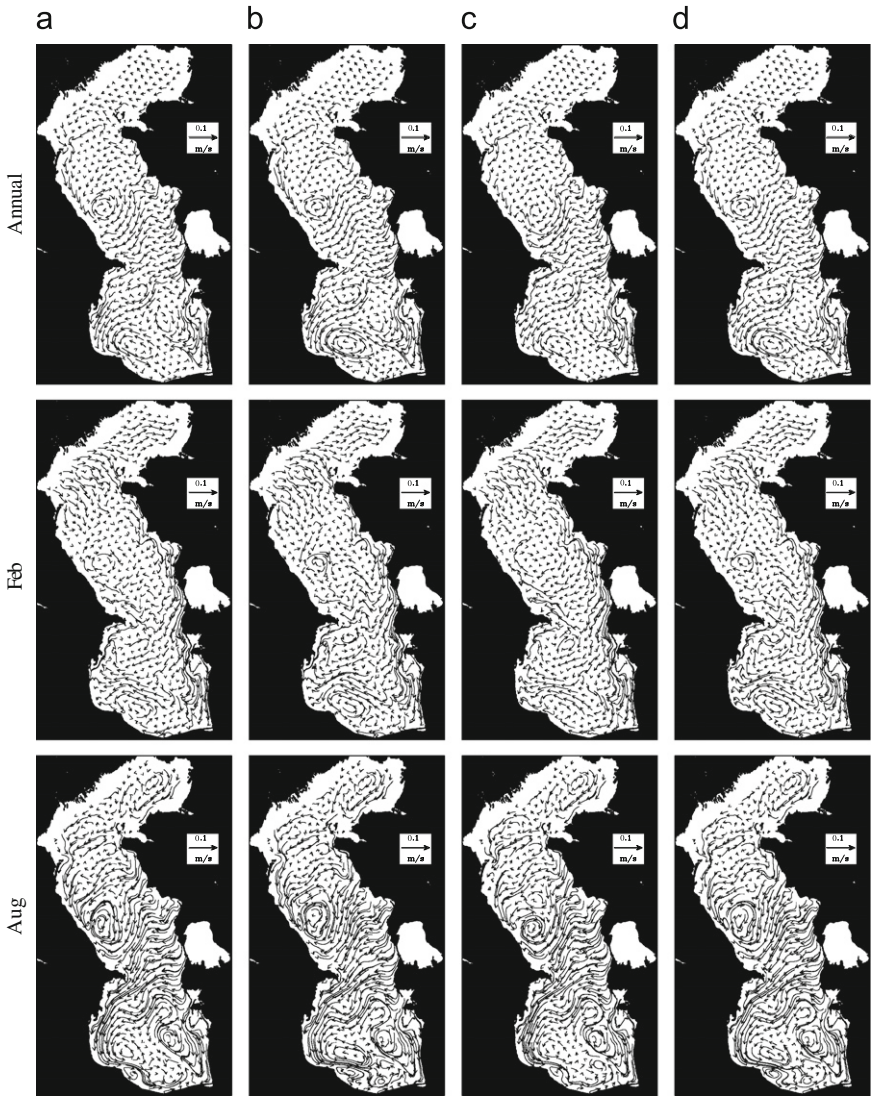

Fig. 10. Surface currents from the 3.3 km resolution climatologically forced Caspian Sea HYCOM simulation. Annual mean currents (i.e., climatological mean) along with means in February and August are shown for the simulation experiments 2–5 (see Table 2). The length of the reference velocity vector is 10 cm s^{-1}. The velocity vectors are sub-sampled as in Fig. 8. (a) Default, (b) No P–E, (c) No rivers and (d) No salt flux.

Table 4
The same as Table 3 but correlations are computed between the default simulation and each one the others.

Default	SSS relaxed	No *P–E*	No Rivers	No salt flux
Jan.	0.86	0.91	0.93	0.93
Feb.	0.91	0.94	0.95	0.95
Mar.	0.88	0.91	0.93	0.94
Apr.	0.89	0.92	0.91	0.93
May	0.94	0.96	0.96	0.96
Jun.	0.97	0.98	0.98	0.98
Jul.	0.97	0.98	0.98	0.98
Aug.	0.94	0.95	0.96	0.97
Sep.	0.94	0.94	0.96	0.96
Oct.	0.94	0.95	0.94	0.96
Nov.	0.92	0.93	0.92	0.95
Dec.	0.89	0.91	0.92	0.94
Ann.	0.97	0.97	0.97	0.98

Using a vector correlation, we further examine whether or not surface currents from the simulation that has SSS relaxation (i.e., expt. 1) are different than those from other simulations. Thus, the impact of ignoring SSS relaxation, *P–E* and rivers on the features of surface circulation can be quantitatively identified. The vector correlation is computed based on the monthly means of zonal and meridional components of the surface currents. The correlation is defined as the cosine of the angle between the two set of vectors (e.g., Crosby et al., 1993). Vectors pointing in the same direction have a positive relationship and those pointing in opposite directions have a negative relationship.

The resulting vector correlations are given in Table 3. Correlations for the surface currents between the pairs of the standard simulation and each one of others are generally high (>0.80). This indicates that *P–E*, rivers and salt fluxes do not have a significant impact on the general circulation of the Caspian Sea.

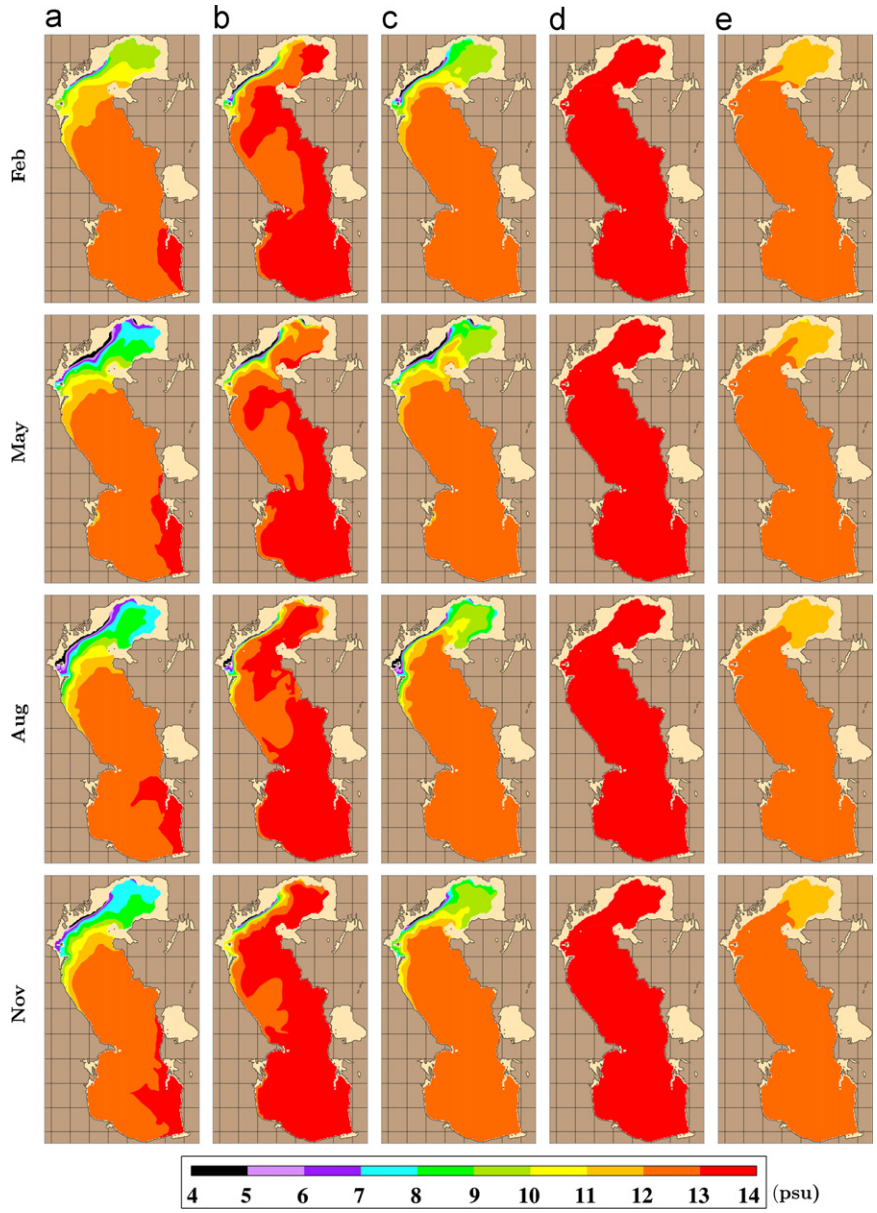

Fig. 11. Monthly mean SSS fields (psu) obtained from the Caspian Sea HYCOM simulations described in Table 2. The results are shown for the selected months of February, May, August and October. (a) SSS relaxed, (b) Default, (c) No P–E, (d) No rivers and (e) No salt flux.

To decide whether or not the correlation values represent a good or poor linear relationship, two statistical tests are applied using the monthly mean surface current values over the seasonal cycle. According to the *t*-test, an absolute value of at least 0.53 is needed for a correlation to be statistically significant in comparison to a correlation value of zero at the 95% ($\alpha = 0.05$) confidence level (Wilks, 1995). For the *z*-test a correlation of 0.7 is used for significance, and a correlation value of even 0.92 is not statistically different from that of 0.7. All correlation values in Table 3 are statistically significant with respect to zero correlation; thus, surface currents from the standard simulation are certainly similar to those from other simulations. All correlations are in fact >0.7, indicating the strong relationship for the surface currents in comparison to the standard simulation. This is true in almost all months. For this reason, we can conclude that evaporation, precipitation, rivers and salt fluxes do not significantly alter the mean variability of surface currents over the Caspian Sea.

To further confirm the results in Fig. 10 which demonstrates little variability in surface currents in the absence of *P–E*, rivers and salt flux, vector correlations for the surface currents are also calculated between the default simulation which has no SSS relaxation and the other three simulations (Table 4). Note that all simulations are identical twins of the default simulation, and the first column in Table 3 is repeated for completeness of the results. Correlations are higher, again indicating that there are not significant changes in the sea surface currents in comparison to the default simulation. In general, the lowest values are noted between the simulations with and without the SSS relaxation in all months. However, they are not generally statistically significant from 0.7 based on the *z*-test.

In addition to the surface currents, the influences of SSS relaxation, *P–E* and rivers on the spatial variability in SSS are investigated in the Caspian Sea (Fig. 11). This is done in February, May, August and November to represent winter, spring, summer and fall, respectively. Comparisons of Fig. 11a and b provide some information about the impact of salinity relaxation. The main effect of the relaxation at the surface is to reduce SSS over the basin in all months. The most significant impact of having the SSS relaxation is evident in the North Caspian Sea where the water is very shallow, and ice cover is large during winter. As mentioned earlier, HYCOM includes a standard energy-loan ice model, which accounts for ice-related processes although a detailed ice validation is beyond the focus of this paper. In the no relaxation case, SSS values of ≈ 9 psu become >14 psu in the northernmost part of the region, a huge increase in comparison to the standard simulation. The reduction in SSS is unrealistic especially in the North Caspian Sea because the standard simulation gives much more accurate results in comparison to observations, as will be further discussed in Section 6, which focuses on model validation.

The only difference between expt. 2 and expt. 3 is that in the latter *P–E* is set to zero (see Table 2). Both simulations include no relaxation to SSS. The effect of not having *P–E* is typically to reduce SSS over the basin (Fig. 11b versus c), and obviously haline buoyancy flux is zero as well. It is already shown in Fig. 9d that the haline buoyancy flux is much smaller than the thermal buoyancy flux in the Caspian Sea. Therefore, the simulation using no SSS relaxation and no *P–E* (i.e., expt. 3) gives a surface salinity field that is nearly identical to the one obtained from the standard simulation of expt. 1 (Fig. 11a versus c).

Similar to the analysis above, a comparison of Fig. 11b versus d provides an insight about the influence of river discharge on SSS. As seen in all months, excluding river effects from the model simulation by setting the discharge rates to zero results in more saline water in the Caspian Sea. Particularly, in the absence of river discharge, SSS does not have much spatial variability, and the river plume near the boundary resulting from the Volga River completely disappears. The simulations having no *P–E* and rivers again reduce SSS (Fig. 11b versus e). This is not surprising because it is already shown in Fig. 11c that zero *P–E* generally reduces the surface salinity and in Fig. 11d that the simulation with no rivers make the region more saline. Thus, the combined effects of both (i.e., expt. 5) give SSS values which are in the middle of the two.

5. Factors controlling the salinity near the Volga River

The Volga River discharging into the northern portion of the Caspian Sea accounts for the majority of inflow into the basin. Thus, in this section a particular focus is given to examination of seasonal variability in SSS in the North Caspian Sea. Climatological annual means reveal very fresh SSS values (<6 psu) near the coastal boundary where the discharge from the Volga River occurs (Fig. 12). There are many small scale features evident from the surface currents even in the annual mean. They generally flow from north to south in the western shelf.

Based on the simulations given in Table 2, we examine the impact of evaporation, precipitation and rivers on the surface salinity in the North Caspian Sea in detail (Fig. 13). Note that the color palette is different than the one in Fig. 11 to better demonstrate SSS values, especially near the coastal boundary. The impact of SSS relaxation is significant along the coastline where the Volga River is discharged into the Caspian Sea (Fig. 13a, b). In comparison to the standard simulation including the SSS relaxation, the low salinity layer of <5 psu on the coastal boundary becomes thinner in May, August and November. However, this layer still exists even when there is no *P–E* (Fig. 13c).

The plume which is mainly caused by the river inflow almost disappears when the discharge from the Volga River is removed,

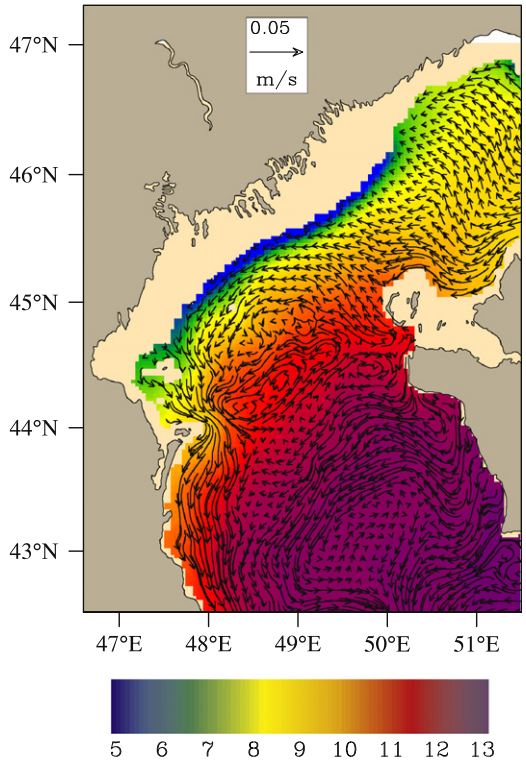

Fig. 12. Annual mean of surface currents overlain on annual mean SSS (psu) in the North Caspian Sea obtained from the 3.3 km resolution Caspian Sea HYCOM. The length of the reference vector is 5 cm s^{-1}. Unlike the earlier figures showing surface currents, all vectors from the model are plotted in this particular region, i.e., they are not sub-sampled.

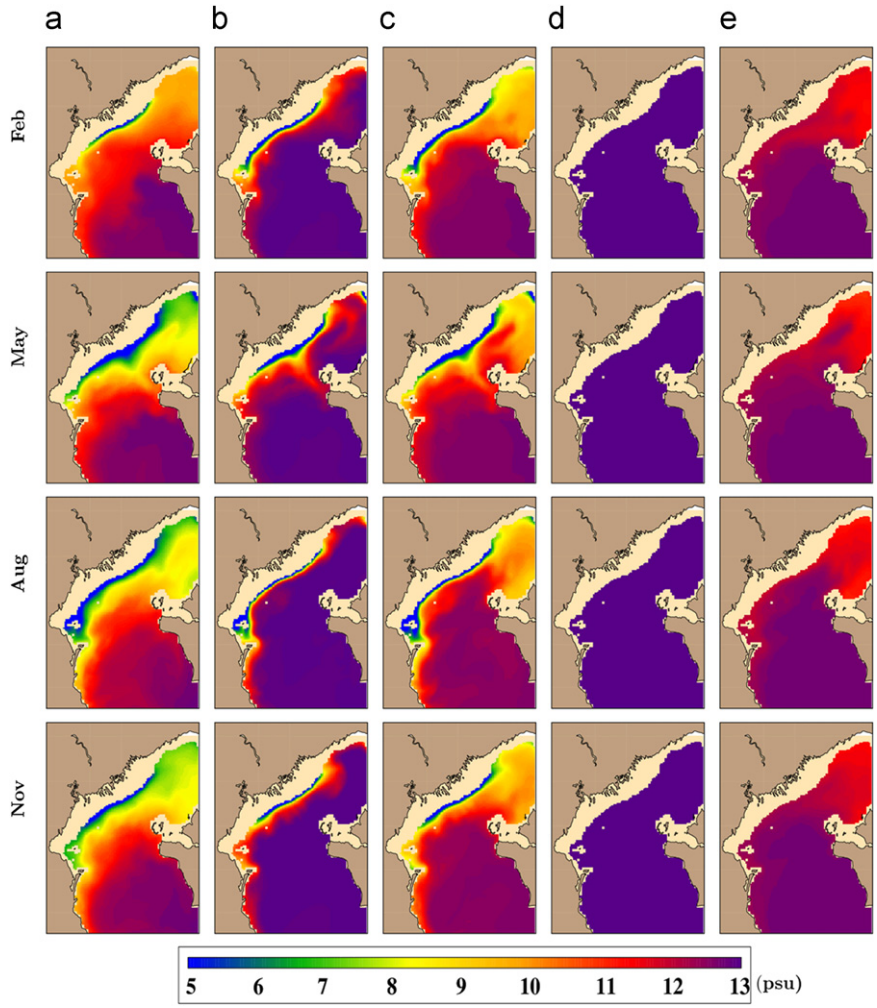

Fig. 13. Monthly mean SSS (psu) fields obtained from the Caspian Sea HYCOM simulations (see Table 2). Seasonal variation of *P–E* and river are included in the default simulation, but relaxation to SSS is excluded. (a) SSS relaxed, (b) Default, (c) No P–E, (d) No rivers and (e) No salt flux.

and this is seen in all months (Fig. 13d). As opposed to the standard simulation with the SSS relaxation, surface salinity completely changes not only on the shelf but also over the entire region, resulting in more saline waters. The low salinity layer near the Volga Rivers does not exist in the simulation performed with no *P–E* and no river discharge. This is due mostly to the impact of river discharge rather than *P–E*.

6. Model validation

In validating results from the Caspian Sea HYCOM, SST and SSS are particularly chosen because their climatological variations are well-observed in the Caspian Sea over the seasonal cycle. For example, spatial variability of climatological monthly mean SSS fields is readily available from the World Ocean Atlas (WOA05). This data set is described in Antonov et al. (2006). Observational data used in WOA05 were averaged by $1^\circ \times 1^\circ$ grids for input to the objective analysis (Boyer et al., 2002). We use $0.25^\circ \times 0.25^\circ$ resolution of this data set, specifically prepared for us by T. Boyer of National Oceanographic Data Center (NODC).

In addition to SSS, monthly SST fields are available from the 4 km resolution Pathfinder data set. The Pathfinder SST climatology was constructed using the same techniques as in Casey and Cornillon (1999) but on the newer $\approx$4 km grid (rather than $\approx$9 km). We specifically use the Pathfinder climatologies for the SST validation since its resolution is close to that of the Caspian Sea HYCOM. The Pathfinder climatology is derived from Advanced Very-High Resolution Radiometer (AVHRR) Pathfinder SST data over 1985–2001. The data processing was done using Infrared (IR) observations from National Oceanic and Atmospheric Administration (NOAA) polar orbiting satellites. A new Pathfinder climatology using 1985–2006 is actively being developed, but it is not available as of this writing. A median filter is applied to fill in the data gaps, and a median smoother is used for the entire field to remove small-scale noise.

In the earlier sections, monthly means were formed for surface currents, heat fluxes, salinity and other variables based on the last 4 (out of 8) model years. Similarly, we construct monthly mean SST climatologies from the model. For example, the climatological mean SSS or SST in January is formed using mean January output from model years 5 through 8. The same process is repeated for the other months. Before evaluation, WOA05 SSS and Pathfinder SST fields are both interpolated to the Caspian Sea HYCOM grid.

For model-data comparisons of SSS and SST two statistical metrics are used: mean error (ME) and root-mean-square (RMS) difference. Let X_i $(i=1,2,\ldots,12)$ be the set of monthly mean WOA05 or Pathfinder observations (reference) from January to December, and let Y_i $(i=1,2,\ldots,12)$ be the set of corresponding HYCOM values (predicted) at a model grid point. Also let $\overline{X}(\overline{Y})$ be the mean of the reference (estimate) values. The statistical

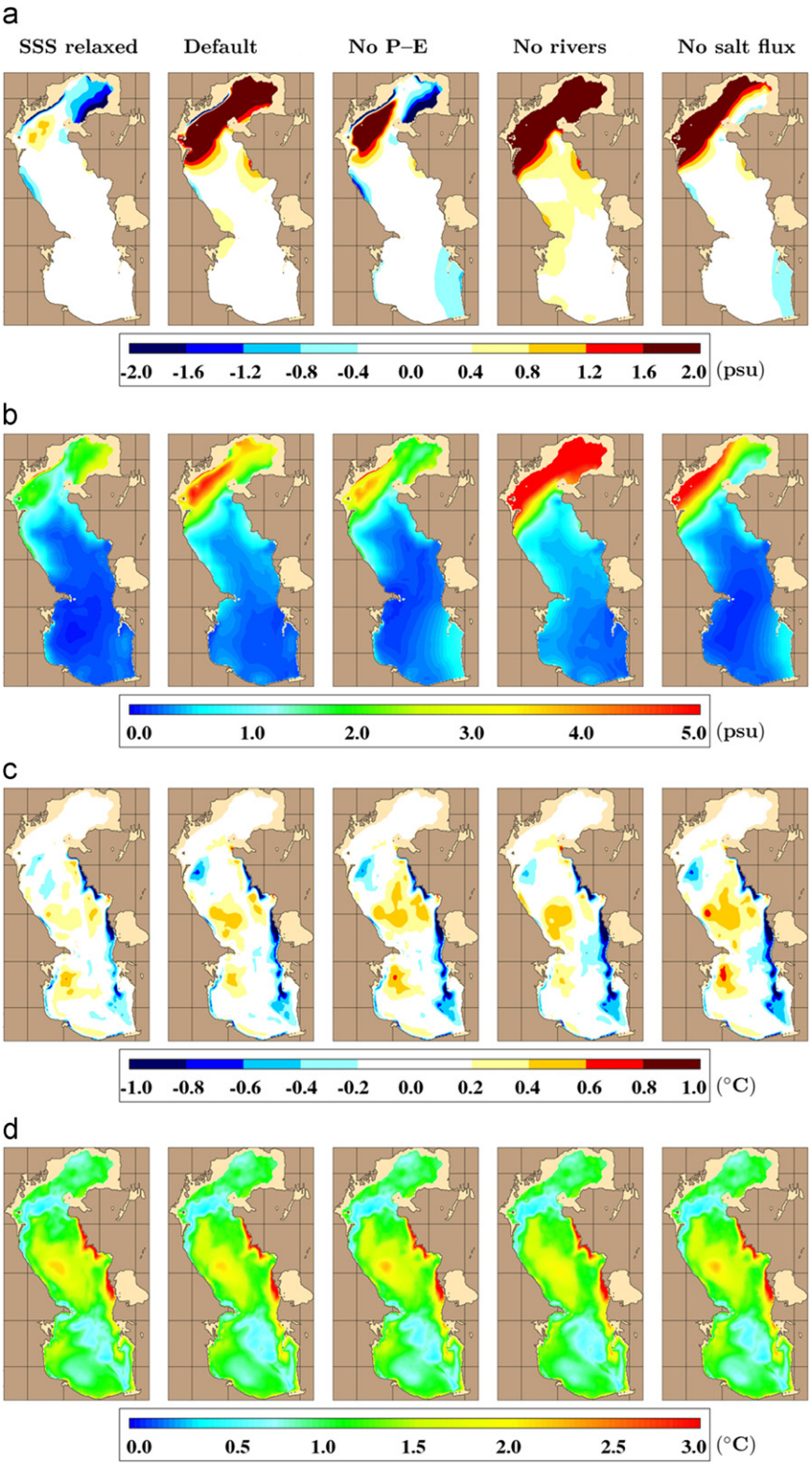

Fig. 14. Statistical validation of climatological monthly mean model SSS and SST calculated over the seasonal cycle. (a) SSS bias: HYCOM-WOA05, (b) RMS SSS difference: HYCOM versus WOA05, (c) SST bias: HYCOM-Pathfinder and (d) RMS SST difference: HYCOM versus Pathfinder.

metrics are then expressed as follows:

$$\mathrm{ME} = \overline{Y} - \overline{X}, \tag{4}$$

$$\mathrm{RMS} = \left[\frac{1}{n}\sum_{i=1}^{n}(Y_i - X_i)^2\right]^{1/2}. \tag{5}$$

Model validation is performed for all simulations listed in Table 2. We first evaluate SSS from the model in comparison to that from WOA05. All simulations give mean SSS bias within ± 0.4 psu in the central and Southern Caspian Sea (Fig. 14a). The main differences arise in the North Caspian Sea. It is clear that the standard simulation results in the lowest mean SSS bias in this

region. The bias in the North Caspian Sea from the default simulation which has no SSS relaxation is much larger than the one which uses SSS relaxation. In addition, too saline waters from the other simulations with respect to the WOA05 climatology are also seen. RMS values can even exceed 4–5 psu in this region, especially for the simulation performed with no rivers (Fig. 14b).

All of the results mentioned in the preceding paragraph clearly point to the importance of *P–E* and rivers in accurate predictions of SSS in the Caspian Sea. Note that at small scales the climatology is not necessarily more accurate than HYCOM because of relatively large sampling bias in a SSS climatology. The model resolves many small scale features which may not exist in a climatology due to its coarse resolution. Rivers and *P–E* do not have significant influences in the other regions as RMS SSS differences are small and similar for all simulations. In particular, the model simulates SSS reasonably well in the Central and South Caspian Sea, with RMS values of <0.4 psu, in general.

Similar to the SSS, spatial variations of ME and RMS values for the model estimates in comparison to the Pathfinder data set are shown in Fig. 14c and d. The most striking feature is that neither *P–E* nor rivers has any significant influence on the monthly SST climatology since bias and RMS values from all experiments are almost identical to each other. Atmospherically forced HYCOM simulations with no assimilation of SST give mean SST bias within $\pm 0.2\,^{\circ}$C in comparison to the Pathfinder climatology over most of the Caspian Sea (Fig. 14c). There are relatively large cold biases of $\pm 1.0\,^{\circ}$C at the coastal boundaries near the eastern Caspian Sea, and these are most likely related to errors in the coarse resolution ERA-40 data used for forcing the model. The overall basin averaged SST bias is almost zero. Thus, the model performs reasonably well even though there is no relaxation to any SST climatology in the simulation.

We should emphasize that the annual climatological SST cycle is built into the model to a limited extent. Including air temperature in the formulations for latent and sensible heat flux (see the Appendix), model SST provides some physically realistic tendency towards the correct SST. If the model SST is too high/low, the flux is reduced/increased relative to that from the correct SST. The trend towards reality is typically not sufficient on its own to keep the model SST on track. Further details can be found in Wallcraft et al. (2008), explaining that the use of the air temperature in a bulk parameterization does not introduce an inappropriate restoring toward observed SST in the model simulations. In other words, the bulk parameterizations in HYCOM imply neither strong damping of SST variability nor strong relaxation to near-surface air temperature.

The success of the Caspian Sea HYCOM in simulating climatological SST is also evaluated using the RMS maps (Fig. 14d). In general, RMS SST values from the standard simulation (generally $1.0\,^{\circ}$C) are not very different from the other simulations. Consistent with the mean bias, RMS values are largest near the eastern boundary. The basin-averaged RMS SST is $1.2\,^{\circ}$C from all simulations. Thus, in comparison to the 4 km resolution satellite-based Pathfinder product, the Caspian Sea HYCOM is able to reproduce climatological monthly mean SSTs with reasonable accuracies. Possible improvements to the relatively coarse atmospheric forcing, as used in this study, are desired especially near the eastern coast where ME and RMS values are relatively large. Another possibility is to set up a fine resolution (e.g., 3 km) resolution atmospheric model in the region, and then obtain atmospheric forcing for the ocean model.

7. Summary and conclusions

The interaction between very shallow coastal waters and the relatively deeper interior region of the Caspian Sea requires an ocean model which has a variety of vertical coordinate systems. In this study this is accomplished by using an eddy-resolving HYbrid Coordinate Ocean Model (HYCOM) in a hybrid $\sigma-z$ model set up. Climatologically forced model simulations are then used for examining seasonal variations of surface variables, with a particular focus on the circulation and salinity.

The Caspian Sea HYCOM revealed the existence of a few permanent eddies, especially in the South Caspian Sea. The fine resolution (3.3 km) also demonstrates some features in the mesoscale circulation which were not previously detected by observations. A series of model simulations indicates that the Caspian Sea surface circulation is not considerably affected by the surface freshwater fluxes alone. It can be deduced from this finding that the combined effect of wind stress and heat flux mainly drives the seasonal variations of the surface circulation in the Caspian Sea. The model simulation performed with no river discharge results in a decrease in intensity of the southward current along the western coast of the central Caspian Sea, explaining the importance of the Volga River for the formation of the current along the western coast of the sea.

Through analysis of monthly mean net and freshwater fluxes along with thermal and haline buoyancy fluxes, significant seasonal variability is noted in the heat fluxes and thereby in the thermal buoyancy fluxes. While the haline buoyancy flux is much smaller than the thermal buoyancy flux, it can have an impact on the spatial and temporal variations of SSS, especially in the North Caspian Sea where the Volga River is discharged. The model simulations also reveal that evaporation, precipitation and salt fluxes have little influence on the climatological mean of monthly SST, but their impact on SSS cannot be ignored in the North Caspian Sea.

Acknowledgments

We would like to thank R. Ibrayev for numerous discussions and data support. Two anonymous reviewers provided helpful suggestions. The numerical HYCOM simulations were performed under the Department of Defense High Performance Computing Modernization Program on a HP/COMPAQ SC45 at the United States Army Engineer Research and Development Center (ERDC), Vicksburg, MS. This research is funded by the Office of Naval Research (ONR) under program element 601153N as part of the NRL 6.1 Global Remote Littoral Forcing via Deep Water Pathways project. This is contribution NRL/JA/7320/08/8235 and has been approved for public release. The co-authors are sad to report that the lead author, A. Birol Kara, passed away on 14 September 2009 at age 39, after battling cancer for a year and a half.

Appendix A. Details of the atmospheric forcing in HYCOM

In addition to wind and thermal forcing, HYCOM forcing incorporates monthly mean climatologies of river discharge and satellite-based attenuation coefficients for Photosynthetically Active Radiation (k_{PAR} in m^{-1}). The shortwave radiation at depth is calculated using a spatially and temporally varying monthly k_{PAR} climatology as processed from the daily-averaged k_{490} (attenuation coefficient at 490 nm) data set from Sea-viewing Wide Field-of-view Sensor (SeaWiFS) during 1997–2001. Thus, using ocean color data, the effects of water turbidity are included in the model simulations through the attenuation depth (k_{PAR}^{-1} in m) for shortwave radiation.

The sum of net shortwave and longwave radiation at the sea surface is so dependent on cloudiness that it is taken directly from ERA-40. The net longwave flux is the sum of downward longwave

(from the atmosphere) and upward black-body radiation. The Numerical Weather Prediction (NWP) (input) black-body radiation is corrected within HYCOM to allow for the difference between NWP SST and HYCOM SST (Kara et al., 2005b). The rate of heating/cooling of model layers in the upper ocean is obtained from the net heat flux absorbed from the sea surface down to a depth, including water turbidity effects (e.g., Kara et al., 2005a). Previously, it was shown that water turbidity can be quite significant in simulations in some ocean basins (e.g., Kara et al., 2004, 2005b).

Latent and sensible heat fluxes at the air–sea interface are calculated using computationally efficient bulk formulae that include the effects of dynamic stability (Kara et al., 2005c). There is no explicit relaxation of the HYCOM SST. However, including air temperature from ERA-40 in the formulations for latent and sensible heat flux automatically provides a physically realistic tendency towards the correct SST.

References

Antonov, J.I., Locarnini, R.A., Boyer, T.P., Mishonov, A.V., Garcia, H.E., 2006. In: Levitus, S. (Ed.), World Ocean Atlas 2005. Salinity, vol. 2. NOAA Atlas NESDIS 62. U.S. Government Printing Office, Washington, DC, 182pp.

Baidin, S.S., Kosarev, A.N. (Eds.), 1986. The Caspian Sea. Hydrology and Hydrochemistry. Nauka, Moscow, 262pp. (in Russian).

Barron, C.N., Kara, A.B., Martin, P.J., Rhodes, R.C., Smedstad, L.F., 2006. Description and application of the global Navy Coastal Ocean Model (NCOM) with examination of vertical coordinate system choices. Ocean Modell. 11, 347–375.

Barron, C.N., Smedstad, L.F., 2002. Global river inflow within the Navy Coastal Ocean Model. In: Proceedings of the Oceans 2002 MTS/IEEE Conference, 29–31 October, pp. 1472–1479.

Bell, M.J., Barciela, R., Hines, A., Martin, M., Sellar, A., Storkey, D., 2006. The forecasting ocean assimilation model (FOAM) system. In: Chassignet, E.P., Verron, J. (Eds.), Ocean Weather Forecasting: An Integrated View of Oceanography. Springer, The Netherlands, pp. 397–411.

Bleck, R., 2002. An oceanic general circulation model framed in hybrid isopycnic-Cartesian coordinates. Ocean Modell. 4, 55–88.

Bleck, R., 2006. On the use of hybrid vertical coordinates in ocean circulation modeling. In: Chassignet, E.P., Verron, J. (Eds.), Ocean Weather Forecasting: An Integrated View of Oceanography. Springer, The Netherlands, pp. 109–126.

Bondarenko, A.L., 1993. Currents of the Caspian Sea and Formation of Salinity Fields of the Waters of the North Caspian Sea. Nauka, Moscow, 122pp. (in Russian).

Boyer, T.P., Stephens, C., Antonov, J.I., Conkright, M.E., Locarnini, R.A., O'Brien, T.D., Garcia, H.E., 2002. In: Levitus, S. (Ed.), World Ocean Atlas 2001. Salinity, vol. 2. NOAA Atlas NESDIS 50. U.S. Government Printing Office, Washington, DC, 176pp.

Brydon, D., Sun, S., Bleck, R., 1999. A new approximation of the equation of state for seawater, suitable for numerical ocean models. J. Geophys. Res. 104, doi:10.1029/1998JC900059:1537-1540.

Buch, E., She, J., 2005. Operational ocean forecasting at the Danish Meteorological Institute. Environmental Research, Engineering and Management 3, 5–11.

Casey, K.S., Cornillon, P., 1999. A comparison of satellite and in situ based sea surface temperature climatologies. J. Climate 12, 1848–1863.

Crosby, D.S., Breaker, L.C., Gemmill, W.H., 1993. A proposed definition for vector correlation in geophysics: theory and application. J. Atmos. Oceanic Technol. 10, 355–367.

Domroes, M., Kaviani, M., Schaefer, D., 1998. An analysis of regional and intra-annual precipitation variability over Iran using multivariate statistical methods. Theor. Appl. Climatol. 61, 151–159.

Ferry, N., Remy, E., Brasseur, P., Maes, C., 2007. The Mercator global ocean operational analysis/forecast system: assessment and validation of an 11-year reanalysis. J. Mar. Syst. 65, 540–560.

Gill, A.E., 1982. Atmosphere–Ocean Dynamics. Academic Press, San Diego, CA 662pp.

Halliwell Jr, G.R., 2004. Evaluation of vertical coordinate and vertical mixing algorithms in the HYbrid Coordinate Ocean Model (HYCOM). Ocean Modell. 7, 285–322.

Ibrayev, R.A., Sarkisyan, A.S., Trukhchev, D.I., 2001. Seasonal variability of the circulation of the Caspian Sea reconstructed from normal hydrological data. Izv. Atmos. Ocean. Phys. 37, 96–104.

Kara, A.B., Hurlburt, H.E., Rochford, P.A., O'Brien, J.J., 2004. The impact of water turbidity on the interannual sea surface temperature simulations in a layered global ocean model. J. Phys. Oceanogr. 34, 345–359.

Kara, A.B., Wallcraft, A.J., Hurlburt, H.E., 2005a. A new solar radiation penetration scheme for use in ocean mixed layer studies: an application to the black sea using a fine-resolution hybrid coordinate ocean model (HYCOM). J. Phys. Oceanogr. 35, 13–32.

Kara, A.B., Wallcraft, A.J., Hurlburt, H.E., 2005b. Sea surface temperature sensitivity to water turbidity from simulations of the turbid Black Sea using HYCOM. J. Phys. Oceanogr. 35, 33–54.

Kara, A.B., Hurlburt, H.E., Wallcraft, A.J., 2005c. Stability-dependent exchange coefficients for air–sea fluxes. J. Atmos. Oceanic Technol. 22, 1077–1091.

Kara, A.B., Wallcraft, A.J., Martin, P.J., Chassignet, E.P., 2008. Performance of mixed layer models in simulating SST in the equatorial Pacific Ocean. J. Geophys. Res. 113, C02020 , doi:10.1029/2007JC004250.

Kosarev, A.N., Yablonskaya, E.A., 1994. The Caspian Sea. SPB Academic Publishing, The Hague, Netherlands 259pp.

Kosarev, A.N., Tuzhilkin, V.S., 1995. Climatological thermohaline fields of the Caspian Sea. State Oceanographic Institute, Moscow State University, Moscow (in Russian).

Knysh, V.V., Ibrayev, R.A., Korotaev, G.K., Inyushina, N.V., 2008. Seasonal variability of climatic currents in the Caspian Sea reconstructed by assimilation of climatic temperature and salinity into the model of water circulation. Izv. Atmos. Ocean. Phys. 44, 236–249.

Large, W.G., Danabasoglu, G., Doney, S.C., McWilliams, J.C., 1997. Sensitivity to surface forcing and boundary layer mixing in a global ocean model: annual-mean climatology. J. Phys. Oceanogr. 27, 2418–2447.

Pinardi, N., Allen, I., Demirov, E., De Mey, P., Korres, G., Lascaratos, A., Le Traon, P.Y., Maillard, C., Manzella, G., Tziavos, C., 2003. The Mediterranean ocean Forecasting System: first phase of implementation (1998–2001). Ann. Geophys. 21, 3–20.

Rodinov, S.N., 1994. Global and Regional Climate Interaction: The Caspian Sea Experience. Water Science and Technology Library, vol. 11. Kluwer Academic Publishers.

Shkudova, G.Y., 1973. Calculation of stationary currents of the North Caspian Sea. Proceedings of the State Oceanographic Institute, 115 (in Russian).

Shriver, J.F., Hurlburt, H.E., Smedstad, O.M., Wallcraft, A.J., Rhodes, R.C., 2007. 1/32° real-time global ocean prediction and value-added over 1/16° resolution. J. Mar. Syst. 65, 3–26 , doi:10.1016/j.jmarsys.2005.11.021.

Terziev, F.S., Kosarev, A.N., Kerimov, A.A. (Eds.), 1992. Hydrometerology and Hydrochemistry of Seas. Caspian Sea, vol. VI, Hydrometeorological Conditions, issue 1. S.-Petersburg, Hydrometeoizdat, 359pp. (in Russian).

Uppala, S., et al., 2005. The ERA-40 re-analysis. Quart. J. R. Meteor. Soc. 131, 2961–3012 , doi:10.1256/qj.04.176.

Wallcraft, A.J., Kara, A.B., Hurlburt, H.E., Metzger, J.E., Chassignet, E.P., Halliwell, G.H., 2008. Value of bulk heat flux parameterizations for ocean SST prediction. J. Mar. Syst. 74, doi:10.1016/j.marsys.2008.01.009.

Wilks, D.S., 1995. Statistical Methods in the Atmospheric Sciences. Academic Press, California 467pp.